Structure of Polyelectrolytes in Poor Solvent

Hans Jörg Limbach[1], Christian Holm[1] and Kurt Kremer[1]

[1] *Max-Planck-Institut für Polymerforschung, PO Box 3148, 55021 Mainz, Germany*

PACS. 61.25.Hq – Macromolecular and polymer solutions.
PACS. 36.20.Ey – Polymer molecules - conformation.
PACS. 87.15Aa – Theory and modeling; computer simulation.

Abstract. – We present molecular dynamics simulations on strongly charged polyelectrolytes in poor solvent. The resulting pearl-necklace conformations are analyzed in detail. Fluctuations in the number of pearls and their sizes lead only to small signatures in the form factor and the force-extension relation, which is a severe obstacle for experimental observations. We find that the position of the first peak in the structure factor varies with the monomer density as $\approx \rho_{\mathrm{m}}^{0.35}$ for all densities. This is a qualitative difference to polyelectrolyte solutions in good solvent which scale as $\rho_{\mathrm{m}}^{1/3}$ and $\rho_{\mathrm{m}}^{1/2}$ in the dilute and semi-dilute concentration regime, respectively.

Polyelectrolytes (PEs) are polymers that carry ionizable groups that dissociate ions in aqueous solution. Technical applications range from viscosity modifiers, precipitation agents, superabsorbers to leak protectors [1]. In biochemistry and molecular biology they are of great importance because virtually all proteins, as well as DNA, are PEs.

Many PEs contain a non-polar hydrocarbon backbone, for which water is a poor solvent. Therefore, in aqueous solution, there is a competition between the tendency to precipitate, the Coulomb interaction and the entropic degrees of freedom. This can lead to elongated strings of locally collapsed structures (pearls). Such necklace conformations have been predicted on the basis of scaling arguments in ref. [2] for a weakly charged single chain PE, and have been confirmed by simulations using the Debye-Hückel approximation [2, 3] and with explicit counterions [4]. The formation of the necklace structure is due to the Rayleigh instability of a charged droplet, which leads to a split once a critical charge is reached. The size of the pearls is determined by the balance between electrostatic repulsion and surface tension. The distance between two pearls is governed by the balance of the electrostatic pearl-pearl repulsion and the surface tension. However, there is up to now no clear experimental proof for the existence of necklace chains [5, 6]. Our previous papers [4] dealt with smaller system sizes and showed that necklaces exist also in the presence of counterions and exhibit a variety of conformational transitions as a function of density. The focus of the present paper is to analyze by extensive computer simulations in detail three possible experimental observables, namely the form factor, the structure factor and the force-extension relation, which can be probed by scattering and AFM techniques. Analyzing the fluctuations of necklace structures we find an extended coexistence regime between different necklace structures and broad distributions for the pearl sizes and the pearl-pearl distances that smear out the necklace signatures. In addition we find that the peak in the structure factor of the solution scales proportional to

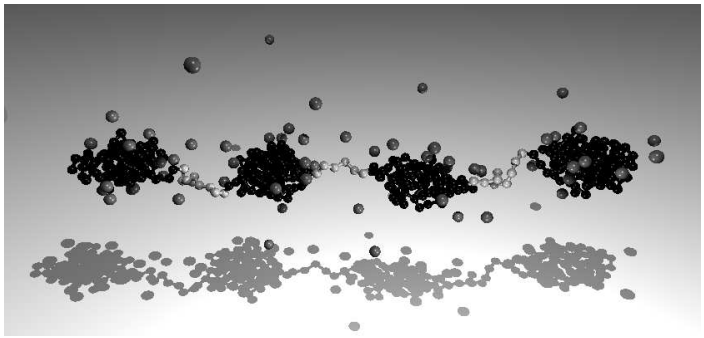

Fig. 1 – Snapshot of a necklace structure analyzed with the cluster algorithm. Chain length $N_{\rm m} = 382$: (black) monomers in pearls, (light gray) monomers in strings, (gray) counterions.

the density $\rho_{\rm m}^{1/3}$ from the dilute up into the dense phase which is in clear contrast to good solvent PEs.

Our PE model is the same as in Ref. [4] and consists of a bead spring chain of Lennard-Jones particles, whose interaction at distance $r < R_c$ is given by $4\,\epsilon[(\frac{\sigma}{r})^{12} - (\frac{\sigma}{r})^6 - c]$, and is zero elsewhere. The constant c is chosen such that the potential value is zero at the cutoff R_c, and ϵ is a measure of the solvent quality. Chain monomers interact up to a distance $R_c = 2.5\sigma$ and experience an attraction with $\epsilon = 1.75\,k_{\rm B}T$. The Θ-point for this model is at $\epsilon = 0.34 k_{\rm B}T$ [4]. The counterions interact via a purely repulsive interaction with $R_c = 2^{1/6}\sigma$. The units of length, energy and time are σ, ϵ, and τ, respectively. For bonded monomers we add a bond potential of the form $-14 k_{\rm B}T \ln(1 - (\frac{r}{2\sigma})^2)$, which results in an average bond length $b = 1.09\sigma$. Charged particles at separation $r_{ij} = |\mathbf{r_j} - \mathbf{r_i}|$ interact via the Coulomb energy $k_{\rm B}T\ell_{\rm B}q_iq_j/r_{ij}$, with $q_i = 1, (-1)$ for the charged chain monomers (counterions). The Bjerrum length $\ell_{\rm B} = e^2/(4\pi\epsilon_S\epsilon_0 k_{\rm B}T)$ (e: unit charge, ϵ_0 and ϵ_S: permittivity of the vacuum and of the solvent) is set to $\ell_{\rm B} = 1.5\sigma$. A velocity Verlet algorithm with a standard Langevin thermostat is used to integrate the equation of motion [7] (friction coefficient $\Gamma = \tau^{-1}$, time step $\Delta t = 0.0125\tau$). The Coulomb interaction was calculated with the P3M-algorithm [8], tuned to force accuracies well above the thermal noise level. The central simulation box of length L contained $N_P = 5$, 10 or 32 chains subject to periodic boundary conditions. Each chain consisted of $N_{\rm m} = 48 \ldots 478$ monomers, with a charge fraction $f = 1/3 \ldots 1/2$. Other parameter sets yield qualitatively similar results [9, 10], so that we restrict ourselves here to the above described "generic" system. The simulation time for the longest chains was around 200 times the measured correlation time for the end-to-end distance $R_{\rm E}$ and the chains centers of mass diffused at least several radii of gyration $R_{\rm G}$. The pressure p is always positive and the pV diagram is convex at all densities, thus our simulations are stable, reach true thermal equilibrium, and reside in a one phase region. The volume density inside the pearls does not exceed 0.47, which is well below the glass transition.

Being first interested in single chain properties we used a monomer density $\rho_{\rm m} = \frac{N_P N_{\rm m}}{L^3} = 1.5\times10^{-5}\sigma^{-3}$. A typically 4-pearl (and 3-string) structure is shown in fig. 1. The substructures contain 90-8-94-6-77-9-98 monomers. For the identification of the pearls and strings we used an especially adapted cluster algorithm [9, 10]. For chains of length $N_{\rm m} = 430$, we find structures with 4, 5, 6 and 7 pearls and an average pearl number $n_{\rm P} = 5.22$. Results for other chain lengths can be found in table I. The coexistence regime between different structure types enlarges with increasing chain length. One reason for the small differences in the free energy is

TABLE I – *Basic observables for various chain lengths at $\rho_m = 1.5 \times 10^{-5}\sigma^{-3}$. Symbols: Chain length N_m, end-to-end distance R_E, average number of pearls n_P, distance between neighboring pearls r_{PP}, number of monomers g_P in a pearl, pressure p and the osmotic coefficient Π. Types denotes the observed structures with n_P pearls, and δr_{PP} and δg_P denote the relative standard deviations. All systems had a Bjerrum-length $\ell_B = 1.5\sigma$ and a charge fraction $f = 1/3$.*

N_m	R_E $[\sigma]$	n_P	Types	$r_\mathrm{PP}[\sigma]$	δr_PP	g_P	δg_P	$p[10^{-6}k_\mathrm{B}T\sigma^{-3}]$	Π
46	3.48	1.0	1	-	-	48	0.0	4.79	0.96
142	12.9	1.97	2	11.6	0.16	67.5	0.17	2.97	0.59
238	25.4	2.89	2 - 4	12.8	0.20	75.5	0.30	2.31	0.46
334	30.4	3.94	3 - 5	13.1	0.21	78.6	0.33	2.0	0.40
382	45.4	4.53	3 - 6	13.3	0.22	78.0	0.32	1.75	0.35
430	55.4	5.22	4 - 7	13.2	0.22	75.3	0.35	1.78	0.36
478	79.7	5.60	4 - 7	13.3	0.21	78.3	0.34	1.76	0.35

the interplay between the chain conformation and the counterion distribution. Conformations with a lower number of pearls have a smaller extension, e.g. R_E, and a larger pearl size. This leads to a stronger attraction of counterions and yields a smaller effective charge on the chain which in turn stabilizes larger pearl sizes and smaller chain extensions. In contrast to scaling theories [11–14] we do not find a collapse into a globular state due to this effect. This is consistent with a more refined theoretical analysis [15] that takes prefactors and finite concentrations into account. The interplay between counterion distribution and structural changes of the conformation can be measured e.g. via the number of counterions $n_c(n)$ for a n pearl structure inside a shell of 3σ from the chain. For example, for $N_\mathrm{m} = 430$ we find $n_c(4) = 60.4$, $n_c(5) = 56.7$, $n_c(6) = 52.8$ and $n_c(7) = 50.2$. From the probability $p(n)$ of finding a n pearl structure we calculate the free energy difference $\Delta\mathcal{F}^{nm} = k_\mathrm{B}T \ln\left(p(n)/p(m)\right)$. For $N_\mathrm{m} = 430$ we find $\Delta\mathcal{F}^{45} = -1.33k_\mathrm{B}T$, $\Delta\mathcal{F}^{56} = 0.66k_\mathrm{B}T$, $\Delta\mathcal{F}^{67} = 1.90k_\mathrm{B}T$. All values are of the order $k_\mathrm{B}T$ which is consistent with the observed large coexistence regime. In order to exclude the possibility of metastable states, we have observed the time evolution for a single chain. We find typically many transitions between different structure types, see i.e. one example for $N_\mathrm{m} = 430$ in fig. 2. Not only the pearl number, also the position and size of the pearls fluctuate strongly. For chains with more than 2 pearls, both the mean values as well as the relative standard deviations δ of the distance r_PP between neighboring pearls and the number g_P of monomers in a pearl are almost constant, see table I, which is consistent with scaling theory.

Scattering experiments probe the conformation via the chain form factor $S_1(q)$ given by

$$S_1(q) = \frac{1}{4\pi N_\mathrm{m}} \left\langle \sum_{i,j=1}^{N_\mathrm{m}} \frac{\sin(q\, r_{ij})}{q\, r_{ij}} \right\rangle, \tag{1}$$

where $\langle \ldots \rangle$ denotes the ensemble average. Fig. 3 shows the measured form factor for $N_\mathrm{m} = 382$ (see table I). In the Guinnier regime ($R_\mathrm{G}q \ll 1$) the radius of gyration R_G can be calculated from $S_1(q) = N_\mathrm{m}\left(1 - (R_\mathrm{G}q)^2/3\right)$, giving $R_\mathrm{G} = 16.8\sigma \pm 0.3\sigma$, in agreement with the directly calculated value $R_\mathrm{G} = 16.9\sigma \pm 0.4\sigma$. In the range $0.07\sigma^{-1} \leq q \leq 0.3\sigma^{-1}$ S_1 scales as $q^{-0.93}$ which corresponds to a stretched object. Around $q = 0.46\sigma^{-1}$ the form factor has an inflection point. A comparison with the intra pearl scattering reveals that this is due to inter pearl scattering (inset in fig. 3). Dividing out the intra pearl form factor gives access to the inter pearl scattering and thus r_PP. The form factor yields $r_\mathrm{PP} = 13.6\sigma$, in accord

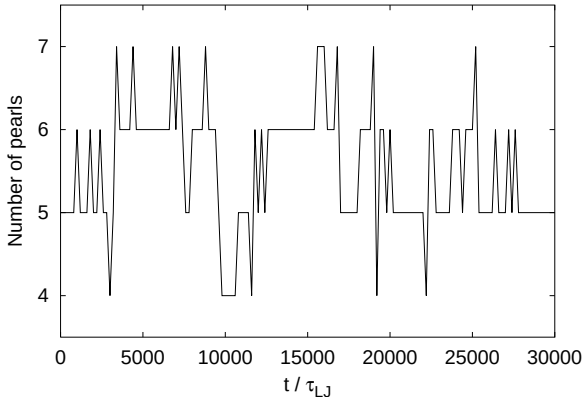

Fig. 2 – Time evolution of a single chain of length $N_{\rm m} = 430$ in equilibrium, shown over a quarter of the physical running time. Many transitions between different structure types can be observed.

with the directly measured value $r_{\rm PP} = 13.3\sigma$ (table I). In the region around $q = 1.0\sigma^{-1}$ we find $S_1(q) \propto q^{-4}$, the typical Porod scattering. From the small dip at $q = 1.7\sigma^{-1}$ one can calculate the radius r_P of the pearls to be $r_P = 2.6\sigma$ which again compares well to the real space value $r_P \simeq 3\sigma$. We conclude that the cooperative effect of fluctuations on overlapping length scales broadens all characteristic signatures which can be revealed by scattering under experimental conditions (polydispersity, charge fluctuations, etc). Thus necklaces might be difficult to detect.

The overall scattering function $S(q)$ of the solution contains additional experimental information. We analyze here the inter chain scattering $S_{IC} = S/S_1$. For good solvent PEs experiments [16], theory [17], and simulations [18] find a pronounced first peak of S_{IC} at $q^* = (2\pi)/\xi$, where ξ is the correlation length. The position varies as $q^* \propto \rho_{\rm m}^{1/3}$ in the very

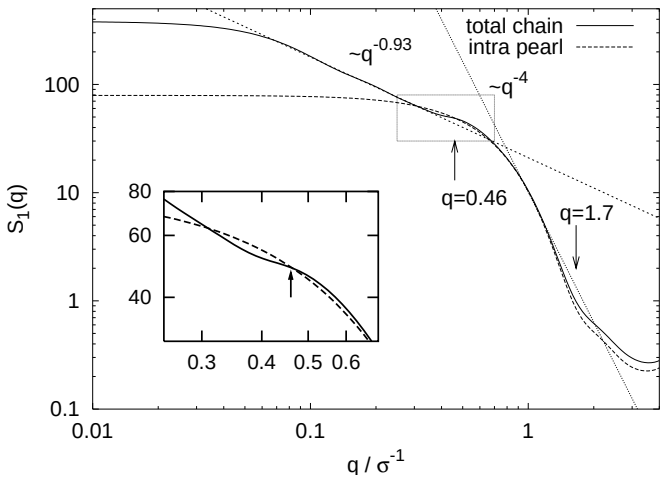

Fig. 3 – Form-factor $S_1(q)$ for pearl necklaces: (solid) form-factor of the whole chain, (dashed) form-factor due to intra pearl scattering, (dotted) fits. The marked region is enlarged in the inset.

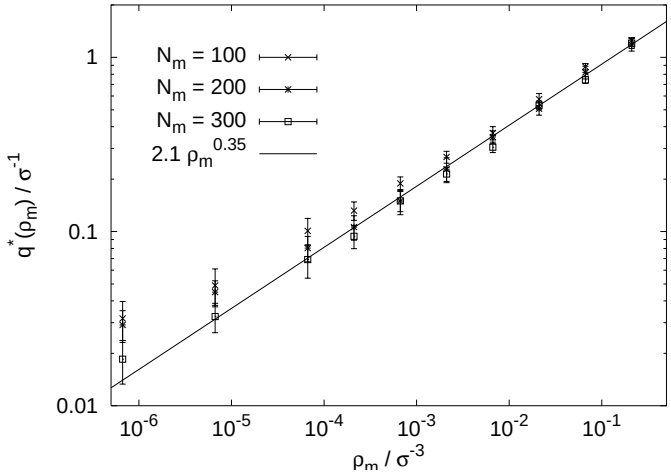

Fig. 4 – Density dependence of the peak q^* in the structure factor for three different chain length $N_\mathrm{m} = 100, 200, 300$ with $f = 0.5$. The black line is a fit to the data with $N_\mathrm{m} = 200$.

dilute regime and crosses over to a $\rho_\mathrm{m}^{1/2}$ regime at higher concentrations. In fig. 4 we have plotted the density dependence of q^* in poor solvent for different chain lengths. Within the error bars we find that for poor solvent chains q^* scales proportional to $\rho_\mathrm{m}^{0.35\pm0.04}$ for *all* concentrations and chain lengths. Possible reasons for this are that the response of the polyelectrolyte conformation to density changes is much larger in the poor solvent case [4,9] than in the good solvent case [18], and the chain extension behaves non-monotonic as a function of density [4,9]. Furthermore, in the density regime between $\rho_\mathrm{m} = 10^{-2}\sigma^{-3} \ldots 10^{-4}\sigma^{-3}$ the chain extension and the pearl number varies most, and almost all monomers are located within the pearls. Upon approaching the dense regime, the string length tends to zero and we find a chain of touching pearls, indicating that the conventional necklace picture breaks down. Our result is compatible to scaling exponents found in scattering experiments [19].

Scaling theories [12, 20] have predicted a $\rho_\mathrm{m}^{1/2}$ regime to start at ρ_o^*, which is defined at the density where $R_\mathrm{E} \approx \xi$, and to extend until $\xi \approx r_\mathrm{PP}$ where a bead-controlled $\rho_\mathrm{m}^{1/3}$ regime starts. We find $\rho_o^* \simeq 5 \times 10^{-2}, 10^{-3}, 10^{-4}$ for $N_\mathrm{m} = 100, 200, 300$, and r_PP is equal to ξ between $\rho_\mathrm{m} = 10^{-2}$ and 10^{-1}. One probable reason for our different findings is the strong inter-chain coupling and influence of the counterions on the conformations which are not sufficiently taken into account in the mean field approach. It is not clear at this stage if the $\rho_\mathrm{m}^{1/2}$ regime can be recovered for much longer chain length. In addition we observe that the chains form a transient physical network at $\rho_\mathrm{m} = 0.2\sigma^{-3}$ for $N_\mathrm{m} \geq 200$ which has neither been seen in previous simulations nor predicted by theoretical approaches but is in accord with experimental studies [19]. During the simulation time these networks reconstruct several times, e.g. chains are not trapped.

A different way to measure a necklace signature can be obtained by single-molecule force spectroscopy, e.g. stretching the chain by AFM [21] or optical tweezers. The case of an imposed end-to-end distance was investigated in Refs. [13, 22, 23] for a weakly charged chain at infinite dilution, for which a saw-tooth pattern in the force-extension curve was predicted. We performed simulations in the weak coupling limit, using a single chain with $N_\mathrm{m} = 256$, $f = 1$, $\ell_\mathrm{B} = 0.08\sigma$, and no counterions present. At equilibrium this system is in a two-pearl

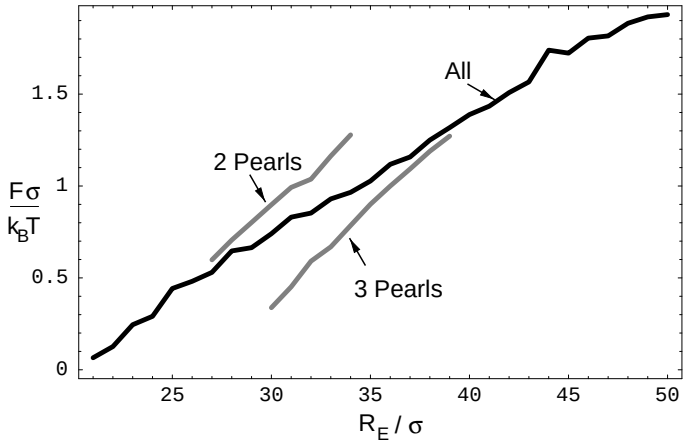

Fig. 5 – Force-extension relation for a transition from two to three pearls. Shown are the average over all conformations, over only two-pearl configurations and only three-pearl configurations.

configuration with $R_{\mathrm{E}} = 21\sigma$. The force-extension curve was obtained by imposing various fixed R_{E} up to $R_{\mathrm{E}} = 50\sigma$. Then the force on the end-monomers was measured, see fig. 5. The first remarkable observation is that the two-pearl state evolves into a three-pearl state under extension, which was predicted in ref. [22,23]. This is counter intuitive from simple arguments, but can be shown to result from the electrostatic inter-pearl interactions [9]. Only when the force averages where computed separately for the three- and two-pearl states, we recognize the predicted saw-tooth pattern in the force. In equilibrium one would expect a rounded plateau for the transition, and the upper and lower part would correspond to metastable superheated and supercooled states. Again, due to the large fluctuations all nontrivial signatures in the force-extension relation are washed out. Analyzing the variance of the measured forces by applying a time window of the order of the transition time we find a 25% increase in the width of the force distribution in the transition region $R_{\mathrm{E}} = 30 \ldots 34\sigma$, and a bimodal force distribution. This means that one needs an experimental time resolution below one μs to directly resolve the structure dependent force difference. An estimate of typical viscous and inertial forces acting on colloidal particles shows that the Brownian motion of small spheres attached to a single PE chain might indeed reflect the fluctuating forces exerted by the chains. The experimental determination of theses fluctuating forces by optical nanorheology [24] or AFM noise analysis [25] presumably is difficult due to the high characteristic frequencies involved.

To sum up we find that poor solvent PEs show an extended coexistence regime between different necklace structures. We observe stable necklaces even with condensed counterions. In all investigated cases the signatures of necklaces in the chain form factor are broadly smeared out. A similar broadening of signatures is found for the force-extension curve which will obscure any of the recently predicted saw-tooth patterns [13, 22, 23]. Nevertheless, the simulations reproduce the predicted initial increase of pearl number under imposing an external length constraint [22, 23]. Our results suggest that the strong fluctuations impose a severe obstacle in observing necklace structures and structural transitions directly in experiments. Finally the location of the first peak in the solution structure factor is qualitatively different from that of PEs in good solvent. This is in good accordance to experiments [19] but does not show the full complexity of the proposed scaling picture at this point [20].

* * *

We thank B. Dünweg, D. Johannsmann, B. Mergell, H. Schiessel and M. Tamashiro for many fruitful discussions and comments. A large computer time grant hkf06 from NIC Jülich is also gratefully acknowledged.

Note: After the submission of this work we learnt that recent light scattering measurements of D. Baigl and C. E. Williams of $q^*(\rho_m)$ for PSS solutions produce an exponent of 0.38 for a charge fraction of 55% which is in good agreement with our simulations.

REFERENCES

[1] *Polyelectrolytes: Science and Technology*, edited by M. Hara (Marcel Dekker, New York, 1993).
[2] Y. Kantor and M. Kardar, Europhys. Lett. **27**, 643 (1994); Phys. Rev. E. **51**, 1299 (1995); A. V. Dobrynin, M. Rubinstein, and S. P. Obukhov, Macromolecules **29**, 2974 (1996).
[3] A. V. Lyulin, B. Dünweg, O. V. Borisov, and A. A. Darinskii, Macromolecules **32**, 3264 (1999); P. Chodanowski and S. Stoll, J. Chem. Phys **111**, 6069 (1999).
[4] U. Micka, C. Holm, and K. Kremer, Langmuir **15**, 4033 (1999). U. Micka and K. Kremer, Europhys. Lett. **49**, 189 (2000).
[5] M. D. Carbajal-Tinoco and C. E. Williams, Europhys. Lett. **52**, 284 (2000); M. N. Spiteri, F. Boue, A. Lapp, and J. P. Cotton, Physica B **234**, 303 (1997).
[6] M. Heinrich *et al.*, Eur. Phys. J. E **4**, 131 (2001); V. O. Aseyev *et al.*, Macromolecules **34**, 3706 (2001).
[7] G. S. Grest and K. Kremer, Phys. Rev. A **33**, 3628 (1986).
[8] M. Deserno and C. Holm, J. Chem. Phys. **109**, 7678 (1998); **109**, 7694 (1998).
[9] H. J. Limbach, Ph.D. thesis, Johannes Gutenberg Universität, Mainz, Germany, 2001. *http://www.mpip-mainz.mpg.de/theory.html*
[10] H. J. Limbach and C. Holm, in preparation (2002).
[11] H. Schiessel and P. Pincus, Macromolecules **31**, 7953 (1998).
[12] A. V. Dobrynin and M. Rubinstein, Macromolecules **32**, 915 (1999).
[13] T. A. Vilgis, A. Johner, and J.-F. Joanny, Eur. Phys. J. E **2**, 289 (2000).
[14] A. Khokhlov, J. Phys. A **13**, 979 (1980).
[15] M. Deserno, Eur. Phys. J. E **6**, 163 (2001).
[16] M. Nierlich *et al.*, J. Physique **40**, 701 (1979); M. Drifford and J.-P. Dalbiez, J. Phys. Chem. **88**, 5368 (1984); K. Kaji, H. Urakawa, T. Kanaya, and R. Kitamaru, J. Physique **49**, 993 (1988); L. Wang and V. Bloomfield, Macromolecules **24**, 5791 (1991).
[17] J. F. Joanny, in *Electrostatic effects in Soft Matter and Biophysics*, Vol. 46 of *NATO Science Series II - Mathematics, Physics and Chemistry*, edited by C. Holm, P. Kékicheff, and R. Podgornik (Kluwer Academic Publishers, Dordrecht, NL, 2001), pp. 149–170.
[18] M. J. Stevens and K. Kremer, J. Chem. Phys. **103**, 1669 (1995).
[19] W. Essafi, F. Lafuma and C. E. Williams, J. Phys. II **5**, 1269 (1995); C. Heitz, M. Rawiso and J. François, Polymer **40**, 1637 (1999); T. A. Waigh, R. Ober, C. E. Williams and J.-C. Galin, Macromolecules **34**, 1973 (2001).
[20] A. V. Dobrynin and M. Rubinstein, Macromolecules **34**, 1964 (2001).
[21] T. Hugel *et al.*, Macromolecules **4**, 1039 (2001).
[22] M. N. Tamashiro and H. Schiessel, Macromolecules **33**, 5263 (2000).
[23] G. T. Pickett and A. C. Balazs, Langmuir **17**, 5111 (2001).
[24] T. Gisler and D. A. Weitz, Curr. Opin. Colloid Interface Sci. **3**, 586 (1998).
[25] M. Gelbert, M. Biesalski, J. Rühe and D. Johannsmann, Langmuir **16**, 5774 (2000).